

Equation (15) is of course valid only if the sample is large enough with respect to the diffusion length of holes to prevent these from diffusing across the crystal to the other side which appears to be the case as shown in Appendix I. The fact that holes do not diffuse across the crystal was used in deriving (15) when  $x_1 \rightarrow \infty$ . Furthermore (11) should hold in the region near the surface from which holes can reach the surface. There is some doubt that this is so for small positive surface potentials. However (11) holds again exactly for a neutral surface.

Numerical integration of (15) yields

$$q = \int_0^{x_1} \frac{D(\alpha + L^{-1})[(K_1/D) + L^{-1} + \gamma^{-1}(\alpha + L^{-1})]}{K_1 \alpha \gamma \exp(\gamma) \int_{\gamma}^{\infty} \exp(-z) dz / z} d\xi, \quad (16)$$

with

$$\gamma = (\alpha + L^{-1}) k_1 / \int_0^{\xi} \frac{\mu_f}{\mu_m} d\xi^+,$$

$\mu_m$  is the electron micromobility and  $\xi^+$ ,  $q$ , and  $\mu_f$  have been defined before.

## Optical Properties of Tellurium and Selenium\*

ROBERT S. CALDWELL† AND H. Y. FAN  
Purdue University, Lafayette, Indiana

(Received December 15, 1958)

The optical properties of tellurium and of trigonal and amorphous selenium have been investigated at wavelengths extending from the intrinsic absorption edge to about 152 microns using polarized radiation. The refractive indices of tellurium and trigonal selenium have been determined from 4 to 14 microns and from 9 to 23 microns, respectively. For amorphous selenium, the refractive index estimated from measured reflectivity shows no appreciable variation from 30 to 152 microns. The temperature shift and the pressure shift of the intrinsic absorption edge in amorphous selenium are found to be  $-1.45 \times 10^{-3}$  ev/°K and  $-2.0 \times 10^{-5}$  ev/atmos, respectively. Lattice absorption bands have been observed in tellurium and selenium; they are attributed to the excitation of combination modes. In tellurium, a strong absorption band has been observed at 11 microns, which is present only for  $E||c$  radiation. The band indicates that there are overlapping branches in the valence band which are separated by about 0.11 ev. The effective mass in the lower branch is estimated to be about four times smaller than that in the upper branch. It is possible that the structure of the valence band is responsible for the high-temperature reversal of the Hall effect in tellurium. The usual carrier absorption increasing smoothly with wavelength has been studied for tellurium using polarized radiations. The effective mass of holes in tellurium has been determined from reflectivity measurements:  $m_{\perp} \sim m_{\parallel} = 0.45 m$  at 300°K,  $m_{\perp} = 0.30 m$  and  $m_{\parallel} = 0.45 m$  at 100°K.

### I. INTRODUCTION

THE investigation of the optical properties of semiconductors has been very fruitful for the understanding of the materials. Tellurium and selenium are two elemental semiconductors, the optical properties of which have not yet been studied as extensively as in some other cases. The fact that these crystals are not cubic in structure and are birefringent makes the optical properties more interesting.

The crystal structure of tellurium consists of parallel spiral chains arranged at the corners and the center of a hexagon. The direction of the chains is the  $c$  axis of the crystal. Every third atom in a chain completes one revolution of the spiral, so that the projection of the atoms on a plane perpendicular to the chain axes consists of equilateral triangles. The distance from an atom to the two nearest neighbors, which are in the same chain, is 2.86 Å, while the distance to the four second nearest neighbors, which are in adjacent chains,

is 3.46 Å. Thus the binding between atoms in a chain is stronger than the binding between the chains with the result that the material cleaves readily parallel to the  $c$  axis. The crystal has  $D_3$  point group symmetry and belongs to the trigonal system. The primitive unit cell contains three atoms.

Selenium can exist in various allotropic forms. The trigonal crystalline form is the most stable and has the same structure as described above for tellurium but with smaller lattice constants, the nearest and second nearest neighbor distances being 2.32 Å and 3.46 Å, respectively. The two other crystalline forms which are monoclinic will not be dealt with in this work. Amorphous selenium, which is fairly stable below 50°C but converts to the trigonal form at higher temperatures, is of interest since it is characterized by the chain structure; x-ray measurements showed that the chain structure persists in the liquid phase of selenium and tellurium.<sup>1</sup>

\* Work supported by a Signal Corps Contract.

† Now at Boeing Airplane Company, Seattle, Washington.

<sup>1</sup> R. C. Buschert, Ph.D. thesis, Purdue University, 1956 (unpublished).

In the present work, optical studies were made on the refractive index, intrinsic absorption edge, and absorption associated with lattice vibrations for tellurium and for crystalline and amorphous selenium. Tellurium crystals doped with different impurity concentrations were investigated with regard to the effect of free carriers. Polarized radiations were used in measuring the crystalline materials in order to study the anisotropy of the optical properties.

## II. EXPERIMENTAL TECHNIQUE

### Sample Preparation

Three methods were used to prepare single crystals of tellurium. The first method, used by Bottom,<sup>2</sup> consisted of slowly cooling a tellurium melt from the top downward. A slow cooling rate was maintained by suspending the pyrex tube containing the melt in a molten bath of  $\text{KNO}_3$ . The second was the Bridgman method and consisted of slowly lowering a vertical tube with molten tellurium through a temperature gradient. With both methods, the maximum diameter of the tube was about 6 mm if single crystals were to be obtained. Often only a portion of an ingot near the center was a single crystal. The direction of the  $c$  axis of the crystal was usually constant in any given ingot but the angle it made with the ingot axis varied from  $0^\circ$  to  $70^\circ$  in different ingots. This situation and the limited diameter of the ingot made it difficult to obtain samples of sufficient areas and thicknesses for accurate absorption measurements. The third method used was the Czochralski method which was successfully applied to tellurium by Weidel<sup>3</sup> and Waldorf.<sup>4</sup> Single crystals were obtained which were 1.5 cm in diameter and 4 or 5 cm long with the  $c$  axis along the direction of growth. The purest crystal grown had an extrinsic hole concentration of about  $5 \times 10^{14} \text{ cm}^{-3}$ , and samples of  $7 \times 10^{17} \text{ cm}^{-3}$  were obtained by doping with antimony.

Single crystals of selenium were prepared by condensation from the vapor phase. A glass tube containing a helium atmosphere and amorphous selenium at the bottom was heated to about  $250^\circ\text{C}$ , allowing the vapor to condense higher up on the inside wall of the tube in a period of several days. Single crystals in the form of flat needles were obtained with the length along the  $c$  axis. Polycrystalline samples were obtained by heating amorphous material at  $205^\circ\text{C}$  for about 24 hours and cooling slowly to room temperature. Optical samples of amorphous selenium were prepared by melting selenium placed between parallel glass plates and quenching to room temperature within a few seconds.

### Measurement Technique

Prism monochromators were used for wavelengths up to 40 microns. Measurements at longer wavelengths were made by using a residual ray apparatus. A grating monochromator which became available during the latter stage of the work was used for a few of the long wavelength measurements.

Polarized radiation was obtained by two different methods: (1) at wavelengths below 25 microns a nine-plate  $\text{AgCl}$  transmission polarizer was used, while (2) at longer wavelengths a single reflection from a polished selenium surface mounted at the polarizing angle was employed. Measurements indicated that both of these methods produced a beam having a proportion of polarization of about 98% exclusive of the effect of the monochromator itself. Generally, the polarizers were placed so as to favor the additional polarization introduced by the monochromators.

## III. ELECTRICAL PROPERTIES OF TELLURIUM

The effect of charge carriers on the optical behavior of tellurium are to be correlated with the electrical properties of the material. It is well known that it has been possible only to prepare tellurium which is  $p$ -type in the extrinsic range. Depending on the concentration of effective acceptors, the Hall coefficient changes its sign to negative at sufficiently high temperatures as the sample becomes intrinsic, due to the higher mobility of electrons as compared to the mobility of holes. With increasing temperature, the Hall coefficient becomes positive again above  $\sim 500^\circ\text{K}$ . The second reversal of sign taking place within the intrinsic region is of particular interest for the understanding of the material.

The samples used had effective acceptor concentrations ranging from  $10^{15}$  to  $10^{19} \text{ cm}^{-3}$ . It was found that the measured resistivity and Hall coefficient were strongly dependent upon the surface conditions of the sample. For a pure single crystal with a cross section of about  $3 \times 1 \text{ mm}$ , the measured apparent resistivity at liquid nitrogen temperature varied from 0.17 to 6.0 ohm-cm. The lowest value was obtained with sand-blasted surfaces while the highest value was obtained with optically polished surfaces. With surfaces ground with carborundum powder, the highest value obtained was 0.5 ohm-cm. Etching in aqua regia gave a value of 4.9 ohm-cm and electroetching gave 3.8 ohm-cm. Another sample which was cleaved from the adjacent region of the same ingot measured 5.0 ohm-cm. The Hall coefficient was also strongly affected by the surface condition, varying from  $286 \text{ cm}^3/\text{coulomb}$  with roughly ground surfaces to  $9910 \text{ cm}^3/\text{coulomb}$  with etched surfaces. These data showed that a high-conductance layer is created by mechanically disturbing the surface. An estimate of the thickness of this layer was obtained by measuring the resistance of the sample as the layer was etched away in steps. Thus it was found that the conducting layer could be about 10 microns

<sup>2</sup> V. E. Bottom, Ph.D. thesis, Purdue University, 1949 (unpublished); Science **115**, 570 (1952).

<sup>3</sup> J. Weidel, Z. Naturforsch. **9a**, 697 (1954).

<sup>4</sup> D. L. Waldorf, M.S. thesis, Purdue University, 1957 (unpublished).

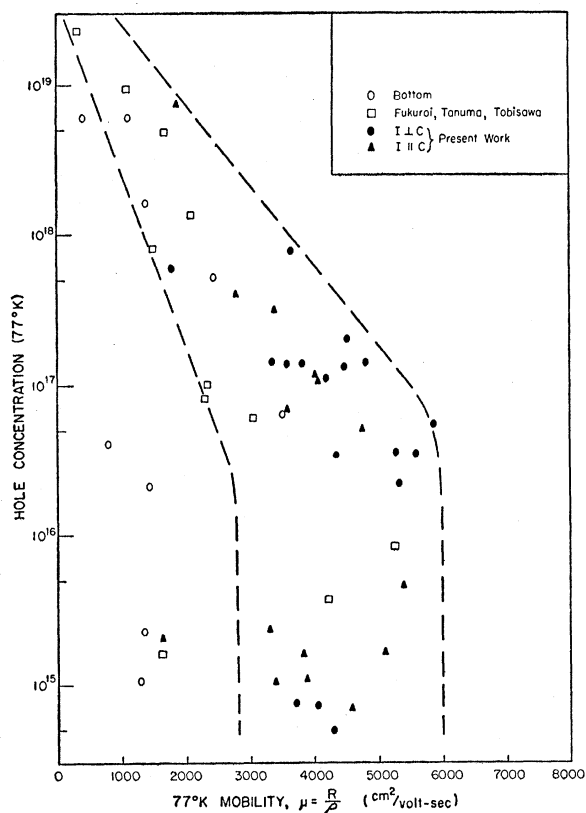


FIG. 1. Hole mobility at 77°K vs hole concentration in tellurium.

thick. The disturbing effect of the surface layer decreases with increasing bulk conductivity and becomes negligible at liquid nitrogen temperature for samples with  $5 \times 10^{16}$  holes/cm<sup>3</sup>. Since optically polished surfaces gave the highest apparent resistivity, about the same as etched or cleaved surfaces, we assume that the optical measurement was not disturbed by surface layers.

The Hall mobility,  $R\delta$ , of holes measured in samples of comparable concentrations of effective impurities varied over a wide range, with current parallel to the  $c$  axis as well as with current perpendicular to the  $c$  axis. The same situation is found in the data reported by other workers<sup>2,5</sup> for polycrystalline samples. Figure 1 illustrates this fact. A similar situation exists in the data for extrinsic samples at room temperature. It has also been observed that repeated measurements made on the same sample at long intervals tended to give higher and higher values of resistivity. Changes up to 20% have been observed without appreciable changes of the Hall coefficient. The cause of these anomalies is not definitely known. One possible explanation is that tellurium crystals may yield readily to stresses. Mechanical handling such as polishing and grinding may affect the sample and internal stress generated during

<sup>5</sup> Fukuroi, Tanuma, and Tobisawa, Science Repts. Research Insts. Tōhoku Univ. A4, 283 (1952).

the growth may be important for the quality of the crystal. Bottom<sup>2</sup> found that tellurium crystals show large asterism in the back reflection spots of x-ray diffraction, indicating the imperfection of the crystals. We have noticed occasionally that, when samples with parallel surfaces were ground down to smaller thicknesses, the surface opposite to that being ground became curved. Also, specimens have been seen to curl noticeably when one face was sandblasted lightly.

A property of particular interest is the ratio of resistivities,  $\rho_{\perp}/\rho_{\parallel}$ , perpendicular and parallel to the  $c$  axis. For samples intrinsic at room temperature, the same value,  $\rho_{\perp}/\rho_{\parallel}=1.9$ , was obtained as found by Bottom.<sup>2</sup> Two methods were used for the measurements. A square sample was used in one of the methods, and the sample was probed along the two perpendicular directions. In the other method, samples with length parallel and perpendicular to the  $c$  axis were cut from a small region of the ingot and then measured separately. The homogeneity of the material is important for the accuracy of the result and the uniformity of the current contacts is also important when a square sample is used. Several samples were measured. The acceptor concentrations of the samples varied from  $10^{16}$  cm<sup>-3</sup> to  $7.5 \times 10^{18}$  cm<sup>-3</sup>. The values of  $\rho_{\perp}/\rho_{\parallel}$  at 77°K ranged from 0.8 to 1.45 with no apparent correlation with the impurity concentration. At room temperature, the values obtained for the extrinsic samples with hole concentrations above  $10^{17}$  cm<sup>-3</sup> varied from 1.4 to 1.8. The average values were  $\rho_{\perp}/\rho_{\parallel}=1.1$  at 77°K and  $\rho_{\perp}/\rho_{\parallel}=1.5$  at room temperature.

#### IV. REFRACTIVE INDEX

The refractive index of tellurium at room temperature has been determined in the wavelength range from 4 to 14 microns by measuring the angle of deviation of a collimated beam of radiation upon passing through an 8°16' tellurium prism. The prism was prepared from tellurium obtained from the Anaconda Company. It was not a single crystal but consisted of several crystallites with boundaries parallel to the  $c$  axis. In the prism used, the  $c$  axis of the crystal was perpendicular to both the refracting edge and the base of the prism. The faces of the prism measured 10×11 mm. The prism angle was measured with an error of less than one minute of arc by using a spectrometer table and the standard autocollimation procedure. The angle of minimum deviation could be determined with an error less than two minutes of arc. The overall error in the refractive index determined from the measurements was estimated to be less than  $\pm 0.015$ . Table I gives the results for radiation polarized parallel and perpendicular to the  $c$  axis. The data are in fair agreement with the earlier results of Hartig and Loferski<sup>6</sup> who obtained values of  $n_{\perp}$  in the 3.9- to 8.0-micron region and values of  $n_{\parallel}$  in the 3.6- to 8.0-micron region. Their values of  $n_{\perp}$  are

<sup>6</sup> P. A. Hartig and J. J. Loferski, J. Opt. Soc. Am. 44, 17 (1954).

about 0.03 higher and their values of  $n_{11}$  are about 0.06 lower than those of the present work. They used the same method with a  $5^\circ$  prism of smaller dimensions than used here. The discrepancy between the two sets of data is slightly larger than the expected errors. We note that if there is a slight variation of the direction of the  $c$  axis in the prism the effect would be to cause the lower index,  $n_1$ , to be too high and the higher index,  $n_{11}$ , to be too low.

The refractive index of trigonal selenium was determined by Kyropoulos<sup>7</sup> to be  $n_1=2.3$  and  $n_{11}=2.8$  at 0.62 micron. By using a reflection method and single crystal needles, Skinner<sup>8</sup> obtained  $n_1=3.0$  and  $n_{11}=4.0$  in the wavelength region 0.4 to 0.65 micron. No results in the infrared region have been reported. In the present work, the refractive index of trigonal selenium was determined by analyzing the transmission interference fringes given by a 50-micron thick needle which had smooth parallel faces. The thickness was measured with an interferometer to within 0.3 micron and this measurement gave the major error in the determination of the refractive index. The transmission measurements were made by using a converging beam of  $12^\circ$  half-angle. The error caused by this procedure was estimated to be only about 0.1%. The measurements made in the 9–23 micron region gave  $n_1=2.78\pm 0.02$  and  $n_{11}=3.58\pm 0.02$  with no appreciable variation.

The refractive index of amorphous selenium at a wavelength of 2.5 microns has been reported to be 2.46 or 2.44 by different authors.<sup>9,10</sup> Values of 2.42 to 2.38 have been reported<sup>11</sup> for the wavelength region from 5 to 15 microns. Using a residual ray spectrometer, we measured the reflectivity of amorphous selenium at wavelengths from 30 to 152 microns. The reflectivity was found to be constant with a value of  $0.175\pm 0.010$ , which corresponds to a refractive index of  $2.44\pm 0.07$ .

### V. INTRINSIC ABSORPTION

Intrinsic absorption is associated with optical excitation of electrons from the valence band to the conduction band. Loferski<sup>12</sup> observed that the long-

TABLE I. Refractive index of tellurium.

Wavelength (microns)	$E \perp c$	$E \parallel c$
4	4.929	6.372
5	4.864	6.316
6	4.838	6.286
7	4.821	6.257
8	4.809	6.253
10	4.796	6.246
12	4.789	6.237
14	4.785	6.230

<sup>7</sup> S. Kyropoulos, Z. Physik **40**, 618 (1926).

<sup>8</sup> C. H. Skinner, Phys. Rev. **9**, 148 (1917).

<sup>9</sup> J. J. Dowd, Proc. Phys. Soc. (London) **B64**, 783 (1951).

<sup>10</sup> E. W. Saker, Proc. Phys. Soc. (London) **B65**, 785 (1952).

<sup>11</sup> L. Henry, Compt. rend. **237**, 148 (1953).

<sup>12</sup> J. J. Loferski, Phys. Rev. **87**, 905 (1952).

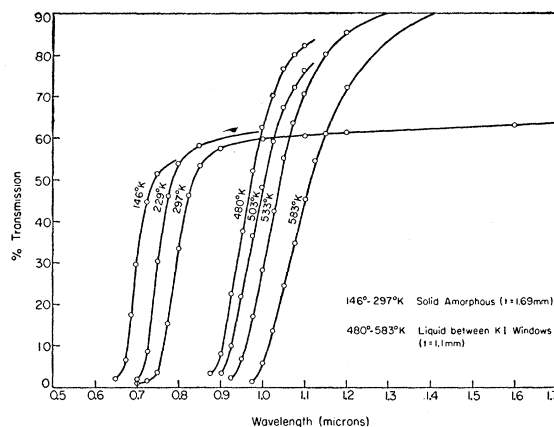


FIG. 2. Transmission curves of liquid and solid amorphous selenium in the region of intrinsic absorption edge.

wavelength edge of the intrinsic absorption in tellurium depends on the direction of polarization of the radiation relative to the  $c$  axis of the crystal, being at longer wavelengths for  $E \perp c$  than for  $E \parallel c$ , e.g., a certain level of transmission corresponds to 3.82 microns for  $E \perp c$  and 3.29 microns for  $E \parallel c$ . The observed behavior indicates that there are overlapping branches in either one or both of the conduction and valence bands. The fact that the two absorption edges are well separated may be taken to indicate that the absorption corresponds to direct transitions. Our transmission measurements on trigonal selenium did not show any appreciable difference in the absorption edge for radiations polarized parallel and perpendicular to the  $c$  axis. For the detection of any small difference more careful measurements have to be made; in particular, the reflectivity of the sample surface must be checked for both directions of polarization.

The transmission curves in Fig. 2 show the variation of absorption edge with temperature for solid amorphous and liquid selenium. The curves for the solid material approach 70% transmission at long wavelengths. This transmission is the maximum possible as limited by reflections corresponding to the refractive index of the material and indicates that absorption loss in the sample was negligible beyond the intrinsic edge. In the case of liquid selenium, the sample was contained in a cell with glass walls. The transmission with the sample in the cell relative to the transmission through the empty cell is plotted. The high level, 95%, reached at long wavelengths again indicates that the absorption in the sample was negligible beyond the intrinsic edge. With the thicknesses of the samples used, the highest absorption coefficient which could be measured accurately was about  $16 \text{ cm}^{-1}$ . In Fig. 3, the photon energy corresponding to this absorption coefficient is plotted against the temperature. The points fall on a continuous straight line for the entire temperature range covering the solid and liquid phases. The result gives  $(\partial E/\partial T)_P = -1.45 \times 10^{-3} \text{ eV}/^\circ\text{K}$ . This value

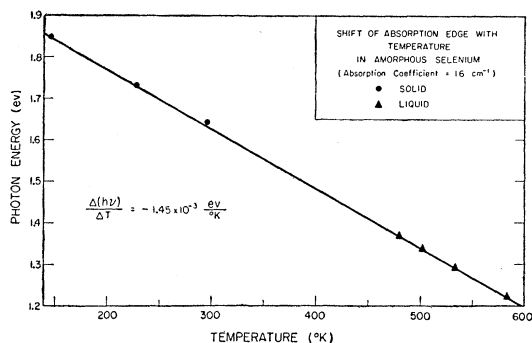


FIG. 3. Intrinsic absorption edge of amorphous selenium as a function of temperature.

agrees with that found by Saker<sup>10</sup> in the range from 300°K to 670°K. The thermal shift observed by Hilsum<sup>13</sup> and Dowd<sup>9</sup> in the range between 86°K and 300°K is about 40% lower than our result. However, these measurements were made on evaporated films and at much higher absorption levels.

The effect of pressure on the intrinsic absorption edge of amorphous selenium is shown in Fig. 4. Pressure was applied to the sample by using nitrogen as the compressing fluid. Correction was made for the effect on the transmission of an increase in the refractive index of nitrogen. The edge shifted to longer wavelengths under pressure which is a behavior similar to that observed in tellurium. A shift of  $(\Delta E/\Delta P)_T$

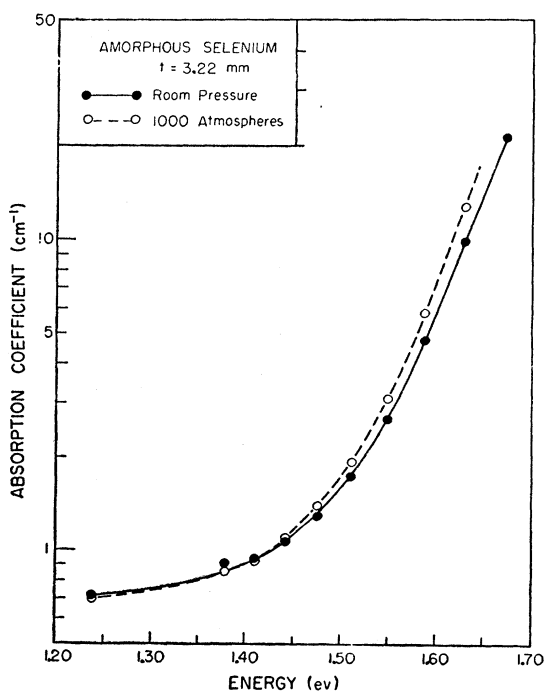


FIG. 4. Intrinsic absorption edges of amorphous selenium at two different pressures.

<sup>13</sup> C. Hilsum, Proc. Phys. Soc. (London) **B69**, 506 (1956).

$= (-2.0 \pm 0.5) \times 10^{-5}$  ev/atmos was obtained for selenium at a level of absorption coefficient of about  $16 \text{ cm}^{-1}$ .

The temperature and pressure coefficients are listed in Table II for amorphous selenium and tellurium. The data for tellurium were obtained by Loferski<sup>14</sup> and Neuringer.<sup>15</sup> The effect of temperature variation may be expressed in the following way,

$$\left(\frac{\partial E}{\partial T}\right)_P = \left(\frac{\partial E}{\partial T}\right)_V - \frac{\beta}{\chi} \left(\frac{\partial E}{\partial P}\right)_T, \quad (1)$$

where  $\beta$  is the volume coefficient of thermal expansion and  $\chi$  is the compressibility. The second term on the right-hand side gives the effect of lattice dilatation. Table II shows that this effect gives a temperature dependence opposite in sign to that observed. A theory for  $(\partial E/\partial T)_V$  has been given by Fan<sup>16</sup> and by Muto and Oyama,<sup>17</sup> attributing the effect to electron-lattice interaction. Using this theory, Fukuroi<sup>18</sup> calculated a value of  $-0.58 \times 10^{-4}$  ev/°K for tellurium. The experimentally deduced value of  $(\partial E/\partial T)_V$  is several times larger in magnitude. However, the energy gap in tellurium and selenium seems to be determined

TABLE II. Energy gap data for tellurium and amorphous selenium.

	$(\partial E/\partial T)_P$ ev/°K	$(\partial E/\partial P)_T$ ev/(kg/cm <sup>2</sup> )	$\beta/\chi$ kg/cm <sup>2</sup>	$-(\beta/\chi)(\partial E/\partial P)_T$ ev/°K	$(\partial E/\partial T)_V$ ev/°K
Se	$-14 \times 10^{-4}$	$-2 \times 10^{-5}$	12.4	$2.5 \times 10^{-4}$	$-16.5 \times 10^{-4}$
Te	$-0.3 \times 10^{-4}$	$-1.9 \times 10^{-5}$	10.1	$1.92 \times 10^{-4}$	$-2.2 \times 10^{-4}$

primarily by the chain structure as evidenced by the following facts: (1) the absorption edge in amorphous selenium varies continuously from the solid to the liquid phase, (2) the absorption edge observed in trigonal selenium at room temperature is very close to the absorption edge in amorphous selenium at the same temperature, and (3) electrical measurement shows that tellurium maintains its energy gap after melting. Thus, it seems that the thermal expansion term should be calculated using the linear coefficient of thermal expansion and compressibility along the  $c$  axis rather than the volume coefficients. For tellurium crystal, both the linear expansion coefficient and the linear compressibility are negative along the  $c$  axis, the ratio being 4.1 atmos/°K instead of 10 atmos/°K for the volume coefficients. The value of  $(\partial E/\partial T)_V$  deduced in this way is reduced to  $-1.1 \times 10^{-4}$  ev/°K, which is much closer to the theoretical estimate.

<sup>14</sup> J. J. Loferski, Phys. Rev. **93**, 707 (1954).

<sup>15</sup> L. J. Neuringer, Phys. Rev. **98**, 1193 (1955).

<sup>16</sup> H. Y. Fan, Phys. Rev. **78**, 808 (1950).

<sup>17</sup> T. Muto and S. Oyama, Progr. Theoret. Phys. (Kyoto) **5**, 833 (1950).

<sup>18</sup> T. Fukuroi, Science Repts. Research Insts. Tôhoku Univ. **A3**, 175 (1951).

## VI. LATTICE ABSORPTION

Transmission measurements were made on tellurium, trigonal selenium and amorphous selenium in the wavelength regions from the intrinsic absorption edges to about 150 microns. In each case, several absorption bands were observed which were apparently associated with the excitation of lattice vibrations. Various samples of each material showed the same bands. In the case of tellurium, which may show carrier absorption, it was ascertained by the use of different samples that the absorption bands in question were independent of the carrier concentration. Figure 5 shows the absorption bands of tellurium and crystalline selenium. These bands, numbered in the sequence of decreasing wavelength, are listed in Table III.

Attempts were made to determine any difference between the absorption bands for radiation polarized

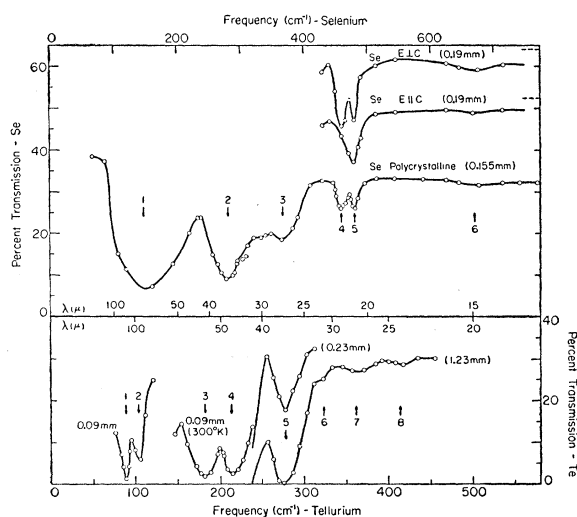


FIG. 5. Transmission curves of tellurium and trigonal selenium, showing lattice absorption bands. Shown are the room temperature data for selenium and 100°K data for tellurium except for one specified case.

with  $E \perp c$  and for radiation with  $E \parallel c$ . For tellurium, it was found that the four short-wavelength bands, 5 to 8, were present with about the same strengths for both directions of polarization. Careful measurements of the bands 3 and 4 showed that these bands were appreciably stronger for the  $E \parallel c$  case than for the  $E \perp c$  case although their positions were independent of the polarization. Using a sample with  $c$  axis perpendicular to the polished surfaces, measurements were made of the long wavelength bands 1 and 2, showing that these bands were present for radiation with  $E \perp c$ . It was not possible to make accurate measurements with polarized radiation to study the  $E \parallel c$  case, due to the weak intensity obtainable at such wavelengths. However, the indication was that the bands 1 and 2 were also present for the  $E \parallel c$  case.

For selenium, measurements made on single crystals

TABLE III. Wavelengths (in microns) of the peaks of the lattice absorption bands in tellurium and selenium.

	Te	Se trigonal	Se amorphous
1	112	70	84
2	95	36	39.5
3	55	27.5	27.2
4	47	21.8	20.4
5	36	20.9	16.1
6	31	15	13.5
7	27.8		
8	24.3		

with polarized radiations showed that band 4 is present only in the  $E \perp c$  case. Measurements on single crystals with polarized radiation were not possible at wavelengths greater than about 23 microns because of intensity losses due to polarization of the beam and the small area of the crystals obtainable.

Since tellurium and trigonal selenium have isomorphous structures it might be expected that their lattice absorption spectra were similar. In fact, a similarity can be seen in Fig. 5 where the frequency scale for selenium has been compressed with respect to the tellurium scale by a factor of 1.33. The bands 1, 2, 3, and 5 in selenium appear to correspond to the bands (1,2), 4, 5, and 7 in tellurium. The frequency ratio of 1.33 is somewhat larger than the square root of the ratio of the atomic masses which has the value of 1.27.

In amorphous selenium, six absorption bands were observed as shown in Fig. 6 and listed in Table III. The bands 3 to 6 were also observed at a low temperature (100°K) and in liquid selenium (493°K). The bands shifted slightly toward lower frequencies as the temperature was raised. In comparing Fig. 6 with the absorption spectrum of polycrystalline selenium in Fig. 5, it might be suggested that the bands 1, 2, 3, and 6 of the two materials mutually correspond while band 4 of the amorphous material corresponds to the double band 4 and 5 of the crystalline phase. However, Table III shows that the frequencies are not sufficiently close for the suggestion to be taken seriously. The effect of the arrangement of neighboring chains is important for the atomic vibrations.

The lattice absorption of a crystal can be explained in terms of the excitation of normal modes or combinations of normal modes of the lattice. The selection rule of excitation requires that the wave number of the mode, or the sum of the wave numbers of the combination of modes, should be equal to the wave number of the radiation, which can be taken as zero since the wavelength of optical or infrared radiation is much longer than the interatomic distance. For the excitation of individual modes, only the fundamental optical modes with zero wave numbers and finite frequencies need be considered. These modes can be obtained by considering a system of points having the point group of the crystal, with the number of points in this system equal to the number of atoms per primitive cell of the

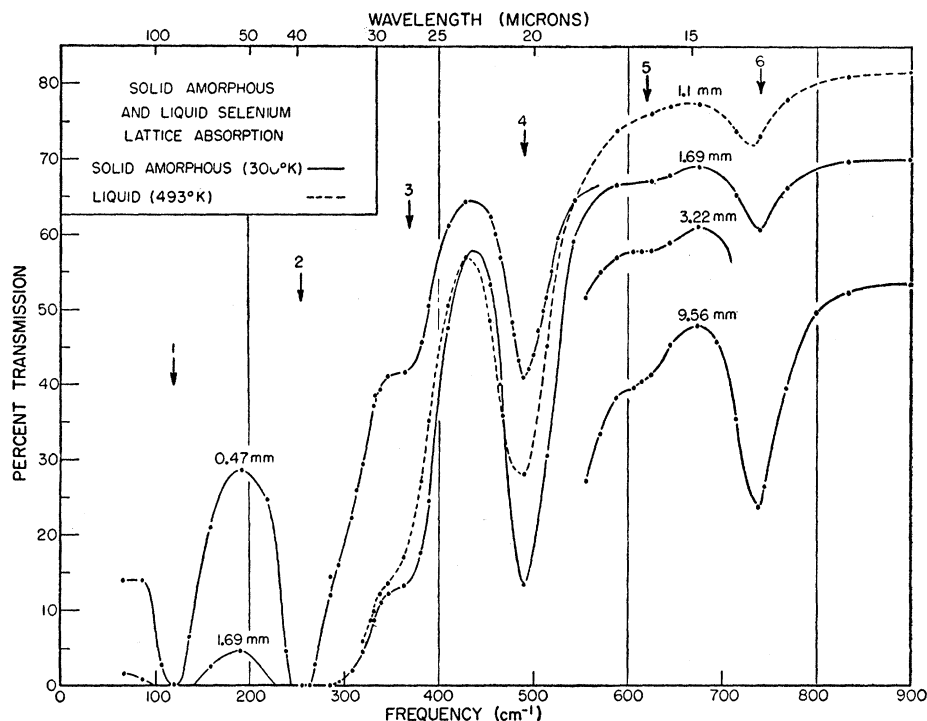


FIG. 6. Transmission curves showing lattice absorption bands in liquid and solid amorphous selenium.

crystal.<sup>19</sup> The structure of tellurium and selenium has the point group  $D_3$  and three atoms per primitive cell. The system of points to be considered is three points at the corners of an equilateral triangle, but the system is to be regarded as having only the symmetry of the  $D_3$  group. A  $D_3$  group has three types of vibrations:  $A_1$ ,  $A_2$ , and  $E$ . The system of three points has one vibration of type  $A_1$ , two of type  $A_2$ , and three of type  $E$ . Of these, the vibrations of type  $A_2$  and two of the vibrations of type  $E$  are translations or rotations of the whole system. However, since the system of points represents a crystal, only the translations are non-genuine vibrations. It follows that there are four genuine vibrations: One each of  $A_1$  and  $A_2$  and two of

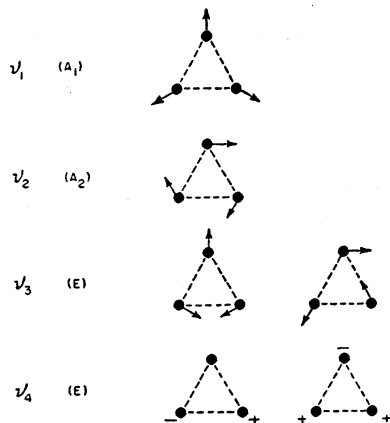


FIG. 7. Normal modes of tellurium lattice. The  $c$ -axis is normal to the plane.

the type  $E$ . The four normal modes of vibration are shown in Fig. 7. Both of the  $E$  modes are doubly degenerate. The  $A_1$  mode should be inactive in the infrared. The  $A_2$  mode can be infrared active only for  $E \parallel c$  whereas the  $E$  modes can be active only for  $E \perp c$ . As mentioned above, none of the absorption bands observed in tellurium showed up only for one direction of polarization. It follows that these absorption bands correspond to combinations of modes instead of individual fundamental modes.

#### VII. FREE CARRIER ABSORPTION

The absorption due to free carriers was investigated with polarized light. The absorption can be studied up to about 35 microns, beyond which strong lattice bands interfere with the determination. Measurements were made on five single crystal samples having extrinsic carrier concentrations in the range  $7 \times 10^{14}$  to  $7.6 \times 10^{18}$   $\text{cm}^{-3}$ . The results for one of the samples are shown in Fig. 8. For radiation with  $E \parallel c$ , there is a pronounced peak near 11 microns. Aside from this peak which is barely noticeable for  $E \perp c$ , there is an absorption which increases smoothly with wavelength. The absorption peak is an indication of the existence of overlapping branches in the valence band and corresponds to interband excitations. The smoothly increasing absorption is the usual free-carrier effect or intraband excitation.

#### Interband Absorption of Holes

The absorption band with peak at 11 microns is due to the presence of holes in the valence band since it is

<sup>19</sup> C. J. Brester, dissertation, Utrecht, 1923 (unpublished); Z. Physik 24, 324 (1924).

present in the extrinsic temperature region where tellurium is *p*-type as well as in the intrinsic region. Besides interband transitions of holes between overlapping branches in the valence band, it might be suggested that the absorption arises from the excitation of valence electrons to localized levels in the energy gap. If the concentration of the localized states is in some way related to the concentration of effective acceptors, such absorption would appear to be tied in with the hole concentration. In order to test this explanation, a sample was measured at a temperature of 200°K in the extrinsic range and at a higher temperature, 373°K, well inside the intrinsic range. If electron transitions to localized levels were the cause, the

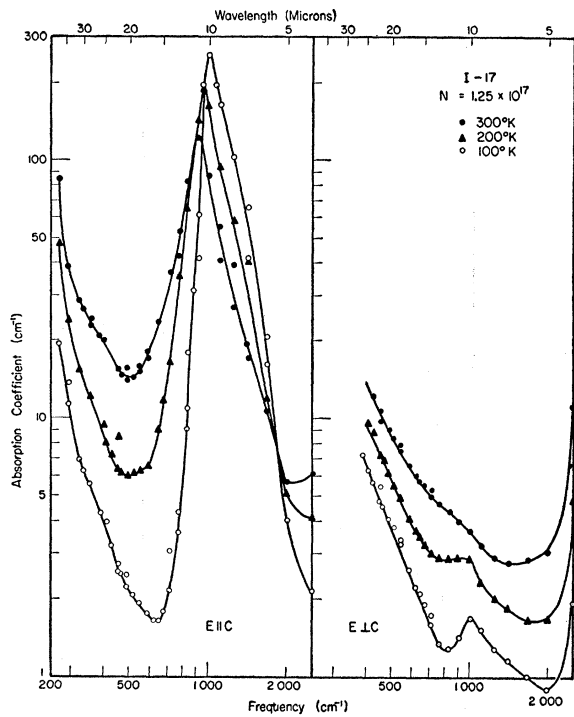


FIG. 8. Absorption coefficient of a tellurium sample at various temperatures, for polarized radiations. The sample is extrinsic with a hole concentration of  $1.25 \times 10^{17} \text{ cm}^{-3}$ .

absorption should be lower at the higher temperature since the levels would be more nearly filled with electrons. The opposite result was observed; the integrated absorption of the 11-micron band was larger by a factor of about seven at the higher temperature. The concentration of free holes deduced from the electrical measurements was also larger at the higher temperature by about the same factor. The observation leaves the interband transition of free holes as the cause of the 11-micron absorption band. The data plotted in Fig. 9 show the proportionality between the integrated absorption of the 11-micron band and the hole concentration in various samples.

The oscillator strength for the transitions involved

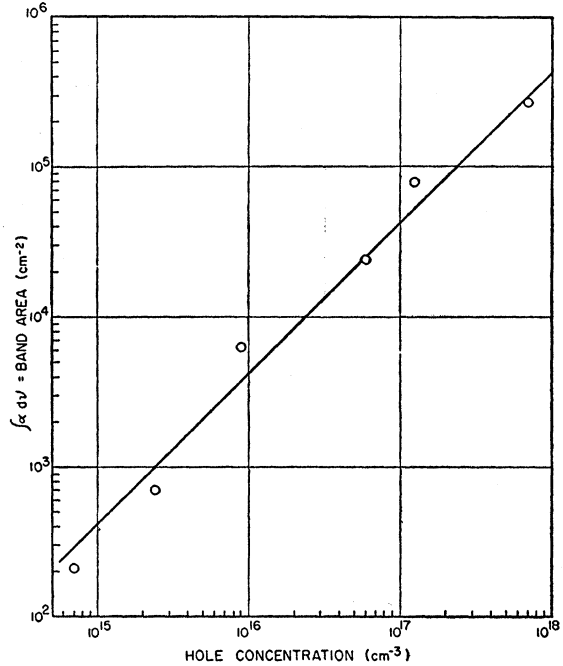


FIG. 9. Integrated absorption of the 11-micron band in tellurium at 100°K vs hole concentration. The straight line corresponds to linear relationship.

can be estimated from

$$f = \frac{n_{11} c m A}{\pi e^2 p} \tag{2}$$

where  $n_{11} = 6.25$  is the refractive index for radiation with  $E \parallel c$ ,  $p$  is the hole concentration, and

$$A = \int \alpha dv \tag{3}$$

is the integrated absorption of the 11-micron band. The data obtained at 100°K gave values of  $f$  varying from 0.8 to 1.0. The high value of oscillator strength indicates that the absorption corresponds to allowed transitions. We are led to a structure of the valence band shown in Fig. 10. Two overlapping bands have their maximum energies at the same point,  $\mathbf{k}_0$ , in the wave vector space. The lower band has a larger curvature corresponding to a lower effective mass as compared to the upper band. The low-frequency threshold of the absorption is determined by the energy separation,  $\Delta E$ , of the energy bands at  $\mathbf{k}_0$ , and the fall-off of the absorption toward higher frequencies reflects the distribution of holes in the upper band. In the case that the two energy bands have spherical constant energy surfaces with effective masses  $m_1$  and  $m_2$ , the absorption due to interband transition can be expressed by

$$\alpha \propto \frac{(h\nu - \Delta E)^{\frac{3}{2}}}{\nu (kT)^{\frac{3}{2}}} \exp \left[ \frac{m_2}{m_2 - m_1} \frac{h\nu - \Delta E}{kT} \right] \tag{4}$$

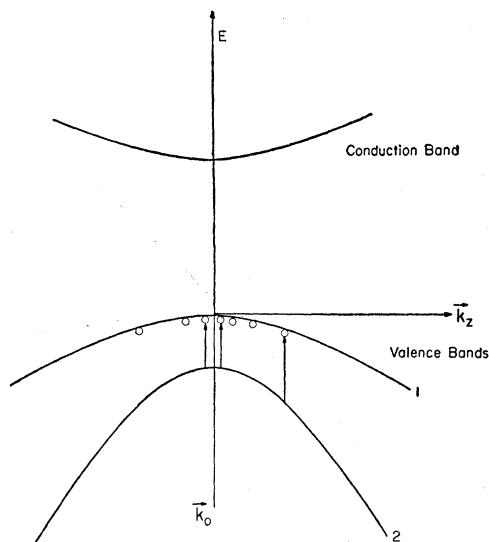


FIG. 10. Energy band diagram for tellurium showing the valence band structure indicated by the 11-micron absorption band.

Figure 11 shows that the experimental data can be fitted reasonably by using this expression with a value of  $m_1/m_2 \approx 4$ .

Reitz<sup>20</sup> calculated the energy bands of tellurium and selenium using a tight-binding approximation and considering only nearest neighbors. Figure 12 shows the energy band structure obtained from the calculation. The minimum of the conduction band and the

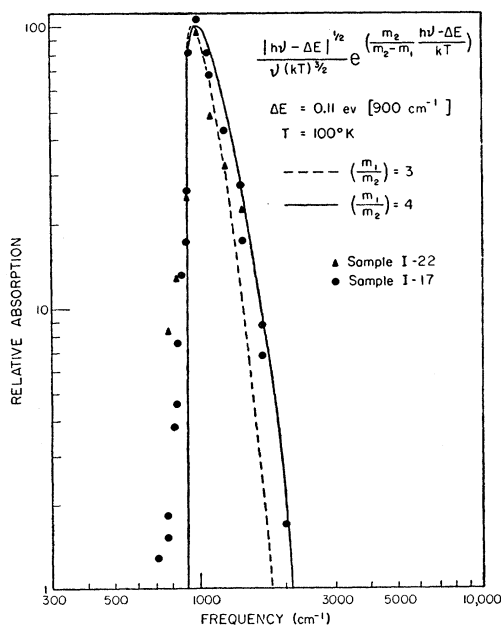


FIG. 11. The 11-micron absorption band, shown normalized, for two tellurium samples of hole concentrations  $7 \times 10^{14} \text{ cm}^{-3}$  and  $1.25 \times 10^{17} \text{ cm}^{-3}$ , respectively. The curves are calculated for inter-band absorption with two different effective-mass ratios.

<sup>20</sup> J. R. Reitz, Phys. Rev. **105**, 1233 (1957).

maximum of the valence band occur at  $k_z = \pi/c$ . There are three  $p$ -bands in the valence band as well as in the conduction band. Optical transitions  $p^- \rightarrow p^-$  and  $p_z \rightarrow p_z$  are forbidden for  $E \perp c$ , and  $p_z \rightarrow p^-$  and  $p^+ \rightarrow p^-$  are forbidden for  $E \parallel c$ . Transitions between the upper two  $p$  levels of the valence band and the lower  $p^-$  level of the conduction band give the absorption edge for the case  $E \perp c$ . Transitions between the  $p^-$  levels of the two bands gives the absorption edge for  $E \parallel c$  which is at higher frequency as was found experimentally. It was not certain from the calculation whether the  $d$  band might not be lowest in the conduction band. With regard to the two absorption edges, this latter case also yields the right answer. In so far as there is a lower branch in the valence band, the calculated band structure is consistent with the deduction based on the observed 11-micron absorption band. However, the 11-micron absorption which would

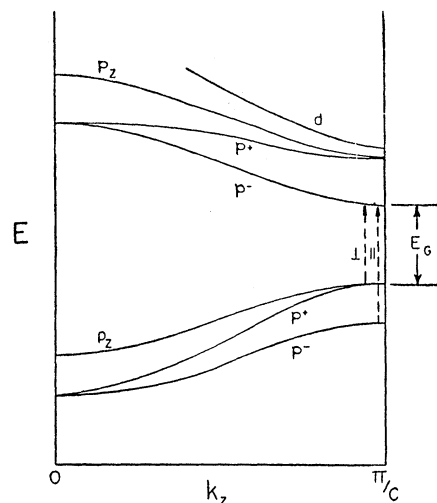


FIG. 12. Energy-band diagram for tellurium according to the calculations of Reitz.<sup>20</sup>

correspond to  $p^- \rightarrow p_z$  or  $p^- \rightarrow p^+$  transitions should be observable with  $E \perp c$  and forbidden for  $E \parallel c$ , in contradiction with the experimental observation.

It has been mentioned above that the Hall coefficient of intrinsic tellurium is negative below  $\sim 500^\circ\text{K}$  and positive above that temperature. The most likely explanation of this effect is that the electron mobility is higher than the hole mobility at low temperatures and becomes lower than the hole mobility above  $500^\circ\text{K}$ . Fukuroi<sup>21</sup> and Callen<sup>22</sup> postulated that this situation is brought about by a decrease of the average electron mobility as a result of an increasing concentration of electrons in a higher conduction band in which the mobility is much smaller than in the lowest conduction band. We note that the valence band structure deduced

<sup>21</sup> T. Fukuroi and S. Tanuma, Science Repts. Research Insts. Tôhoku Univ. **A4**, 353 (1952).

<sup>22</sup> H. B. Callen, J. Chem. Phys. **22**, 518 (1954).

TABLE IV. Carrier absorption in various samples of tellurium.

Hole concentration ( $10^{18} \text{ cm}^{-3}$ )	Absorption cross section ( $10^{-17} \text{ cm}^2$ )				Absorption ratio $\alpha_1/\alpha_{11}$ (at $25\mu$ )		
	$E \perp c$ (at $20\mu$ )		$E \parallel c$ (at $25\mu$ )		$300^\circ\text{K}$	$200^\circ\text{K}$	$100^\circ\text{K}$
	$300^\circ\text{K}$	$100^\circ\text{K}$	$300^\circ\text{K}$	$100^\circ\text{K}$			
6.0		2.2		1.2			2.6
12.5	6.6	3.2	16.8	3.2	0.63	1.14	2.3
69	7.0	4.0	12.0	4.1	0.94	1.27	1.8
760	6.4		12.8		0.85		

from the 11-micron absorption band may be responsible for the sign reversal of Hall coefficient. At the reversal temperature, the Hall coefficient is equal to zero, which requires

$$n\mu_e^2 - p_1\mu_1^2 - p_2\mu_2^2 = 0, \quad (5)$$

where  $\mu$  is carrier mobility and subscripts 1 and 2 refer to the two types of holes. With  $n = p_1 + p_2$ , we get

$$\left(\frac{\mu_2}{\mu_1}\right)^2 = \left(\frac{\mu_e}{\mu_1}\right)^2 + \left[\left(\frac{\mu_e}{\mu_1}\right)^2 - 1\right] \frac{p_1}{p_2}. \quad (6)$$

The ratio of the two types of holes is given by

$$p_1/p_2 = (m_1/m_2)^3 \exp(\Delta E/kT). \quad (7)$$

The ratio,  $\mu_e/\mu_1$ , has been estimated by various authors to be about 1.55.<sup>21,23,24</sup> From the study of the 11-micron absorption band, we get  $\Delta E = 0.11 \text{ eV}$  and  $m_1/m_2 = 4$ . These values yield

$$\mu_2/\mu_1 = 12 \simeq (m_1/m_2)^{1.8}. \quad (8)$$

If the two types of holes are scattered each within its own energy band, we would expect  $\mu \propto m^{-\frac{1}{2}}$ . On the other hand, it is assumed for germanium that the mobility ratio of the two types of holes is inversely proportional to their mass ratio. However, in the latter case the energy bands containing the two types of holes have a common maximum energy. In the present case, the two energy bands under consideration are separated by  $\Delta E$ . The mobility ratio obtained seems not unreasonable. Thus it is possible that the structure of the valence band is responsible for the sign reversal of the Hall coefficient. According to Loferski, the two intrinsic absorption edges, for  $E \perp c$  and  $E \parallel c$ , are shifted relative to each other by about 0.05 eV. If the absorption edges correspond to transitions from the two valence bands to a conduction band, the shift should be equal to  $\Delta E = 0.11 \text{ eV}$ .

#### Intraband Absorption of Holes

The intraband absorption of holes was measured on several samples of different carrier concentrations. Strong lattice bands limited the study to wavelengths less than 35 microns. For  $E \parallel c$  radiation, the strong interband absorption around 11 microns put a lower

<sup>23</sup> Aigrain, Dugas, Legrand des Cloizeaux, and Jancovici, *Compt. rend.* **235**, 145 (1952).

<sup>24</sup> V. A. Johnson, Purdue University Quarterly Report, October 1-December 31, 1952 (unpublished).

limit for the wavelength at about 15 microns. The wavelength dependence of the absorption may be approximately expressed by a power,  $S$ , of the wavelength. For samples of hole concentrations in the range  $10^{17}$  to  $10^{18} \text{ cm}^{-3}$ , the value of  $S$  varied from 2.0 to 2.5 for  $E \perp c$  and from 1.8 to 2.8 for  $E \parallel c$ , as the temperature was lowered from  $300^\circ\text{K}$  to  $100^\circ\text{K}$ . The theory of absorption by free carriers<sup>25</sup> shows that the absorption varies as  $\lambda^{1.5}$  when the carriers are scattered by lattice vibrations and varies approximately as  $\lambda^{3.5}$  when the carriers are scattered by ionized impurities. The results for tellurium are qualitatively consistent with this theory. The effect of ionized impurities should be more dominant at lower temperatures, giving stronger wavelength dependence.

The absorption coefficient reduced to unit hole concentration,  $\alpha/p$ , gives the absorption cross section of holes. The values obtained for various samples are listed in Table IV. The values for  $300^\circ\text{K}$  are in general higher than those for  $100^\circ\text{K}$  and do not show any correlation with the concentration of holes or acceptor impurities. The increase of absorption cross section with temperature shows the effect of lattice scattering which should be independent of the hole concentration. At the low temperature,  $100^\circ\text{K}$ , the absorption cross section is higher for larger hole concentration, showing the effect of scattering by ionized impurities which is related to the hole concentration. The ratio of absorptions,  $\alpha_1/\alpha_{11}$ , is also given in the table. It should be noted that the  $300^\circ\text{K}$  values of  $\alpha_{11}/p$  and  $\alpha_1/\alpha_{11}$  are not very reliable since the 11-micron band absorption at this temperature does not drop very sharply on the long wavelength side, as can be seen in Fig. 8. There may be appreciable contribution from the interband absorption even at 25 microns. The values of  $\alpha_{11}$  calculated from the measured absorption may therefore be too high.

#### Intraband Absorption in the Intrinsic Range

In the intrinsic temperature range, both electron and hole carriers contribute to absorption. The absorption increases with temperature as shown in Fig. 13. For the temperature range under consideration, the effect of lattice scattering should be dominant. In this case, the intraband absorption is proportional to the carrier concentration and the temperature, according to the

<sup>25</sup> Fan, Spitzer and Collins, *Phys. Rev.* **101**, 566 (1956); H. Y. Fan, *Repts. Progr. in Phys.* **19**, 107 (1956).

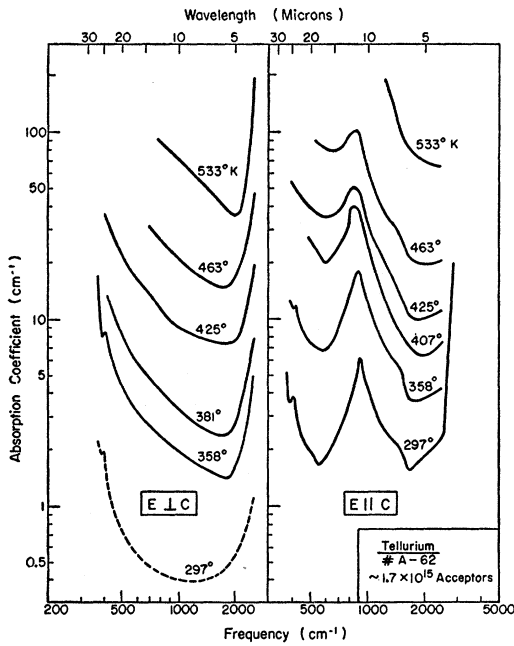


FIG. 13. Absorption coefficient of tellurium at various temperatures in the intrinsic range, for polarized radiations.

theory.<sup>25</sup> By expressing the energy gap in the form

$$E_G = E_{G_0} + aT, \quad (9)$$

$E_{G_0}$  being an appropriate constant for the temperature region, we get

$$\alpha \propto T n_i \propto T^{\frac{3}{2}} \exp(E_{G_0}/2kT), \quad (10)$$

Figure 14 gives the semilogarithmic plot of  $\alpha T^{-\frac{3}{2}}$  against  $1/T$  for a sample in the intrinsic temperature range. The points obtained with  $E \perp c$  radiation can be fitted with a straight line, the slope of which corresponds to  $E_{G_0} = 0.42$  ev. The data for  $E \parallel c$  seem to scatter around a straight line of the same slope; the scatter is due to the fact that the 11-micron absorption made it difficult to determine the intraband absorption accurately. The values of  $E_{G_0}$  estimated by different workers from various types of measurements are considerably lower, being around 0.33 ev. Thus the observed growth of carrier absorption with temperature is faster than expected. We have at present no satisfactory explanation for this phenomenon. It might be suggested that the absorption per carrier increases faster than linearly with temperature, which could be the case if scattering by optical modes of vibration were becoming important.

### VIII. REFLECTIVITY AND CARRIER EFFECTIVE MASS OF TELLURIUM

The effect of free carriers on the infrared reflectivity of semiconductors was used by Fan and Becker<sup>26</sup> to

<sup>26</sup> H. Y. Fan and M. Becker, *Conference on Semiconducting Materials* (Butterworths Publishing Company, London, 1951).

estimate the effective mass of carriers. More recently, the method was given careful consideration by Spitzer and Fan<sup>27</sup> and was applied to a number of semiconductors. The method utilizes the carrier contribution to the electric susceptibility, which is given by

$$\chi_e = -\frac{pe^2}{m\omega^2 + (1/\tau)^2}, \quad (11)$$

where  $p$  is the carrier concentration,  $\omega$  is the angular frequency of radiation and  $\tau$  is an appropriate collision time. An approximate estimate of  $\tau$  can be obtained from the mobility. The tellurium samples used had mobilities of about 400 cm<sup>2</sup>/volt-sec or more at room temperature with considerably higher values at lower temperatures. For  $m = 0.5$  as determined from these experiments, we get

$$1/\tau \approx e/m\mu \leq 1.2 \times 10^{12} \text{ sec}^{-1}. \quad (12)$$

The wavelengths used in the measurements were less than 35 microns, for which  $\omega \gg 1/\tau$ . Thus the effective mass can be calculated from  $\chi_e$  without the necessity of knowing the value of  $1/\tau$ . The susceptibility is related to the optical constants, refractive index,  $n$ , and extinction coefficient,  $k$ , by the relation.

$$\epsilon_0 + 4\pi\chi_e = n^2 - k^2, \quad (13)$$

where  $\epsilon_0$  is the dielectric constant of the material ex-

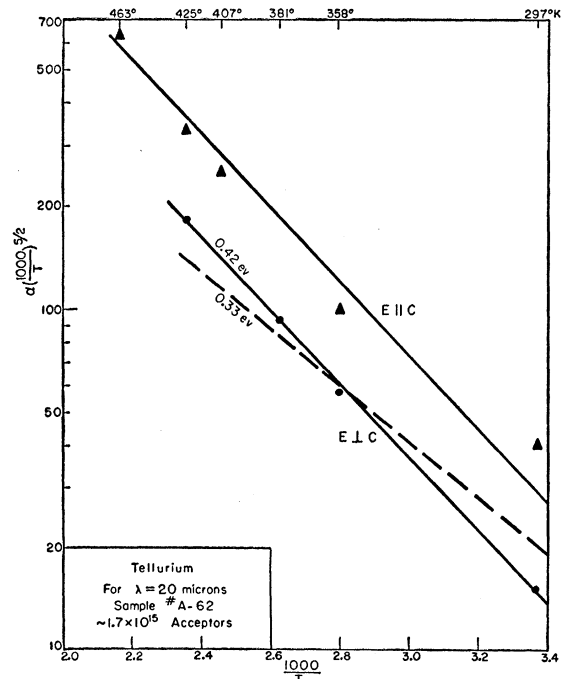


FIG. 14. Product of absorption coefficient and  $(1000/T)^{5/2}$  vs  $1000/T$  for tellurium in the intrinsic temperature range.

<sup>27</sup> W. G. Spitzer and H. Y. Fan, *Bull. Am. Phys. Soc. Ser. II*, 1, 331 (1956).

clusive of the free carrier effect. The optical constants can be determined by measuring the reflection and transmission of the radiation.

Figure 15 shows the reflectivity curve for two of the samples measured. For these measurements the samples used were sufficiently thick to give negligible transmission. The reflectivity is related to the optical constants by the expression

$$R = \frac{(n-1)^2 + k^2}{(n+1)^2 + k^2} \quad (14)$$

The variation of reflectivity on the short-wavelength side of the pronounced minimum is determined mainly by the refractive index, the value of  $k^2$  being negligible. This is normally the case. The validity of the assumption was also verified by transmission measurements made on one of the samples which was polished down to a suitable thickness.

By neglecting  $k$ , values of  $\chi_e$  were calculated from the measured reflectivity according to (13) and (14). The values varied approximately as the square of the wavelength in agreement with (11). The results for radiations polarized parallel and perpendicular to the  $c$  axis gave the following effective mass parameters:

- at 300°K:  $m_{\perp} \simeq m_{\parallel} \simeq 0.45 m$ ;
- at 100°K:  $m_{\perp} \simeq 0.30 m$ ,  $m_{\parallel} \simeq 0.45 m$ .

The accuracy of these results was estimated to be about 10%. The low-temperature measurements were made only on one of the samples with a hole concentration of  $9 \times 10^{18} \text{ cm}^{-3}$ .

The ratios of dc conductivities, intraband carrier absorptions, refractive indices, and effective masses, for electric fields parallel and perpendicular to the  $c$  axis, are related. According to the theory of carrier

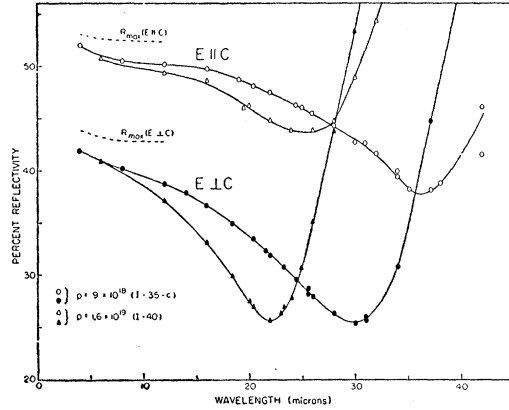


FIG. 15. Reflectivity vs wavelength for polarized radiations. Curves are shown for two antimony-doped tellurium samples, with hole concentrations  $9 \times 10^{18} \text{ cm}^{-3}$  and  $1.6 \times 10^{19} \text{ cm}^{-3}$ , respectively.

absorption,<sup>25</sup>

$$\alpha = 4\pi\sigma/cn \propto \sigma_0/n\tau^2, \quad (15)$$

where  $\sigma_0$  is the dc conductivity. With  $\sigma_0 \propto \tau/m$ , we get

$$\alpha \propto [n\sigma_0 m^2]^{-1}. \quad (16)$$

Hence

$$\frac{m_{\perp}}{m_{\parallel}} = \left( \frac{n_{\parallel} \alpha_{\parallel} \rho_{\perp}}{n_{\perp} \alpha_{\perp} \rho_{\parallel}} \right)^{\frac{1}{2}}. \quad (17)$$

At 100°K, the average value of  $\rho_{\perp}/\rho_{\parallel}$  is 1.1 and the average value of  $\alpha_{\perp}/\alpha_{\parallel}$  in Table IV is about 2.2. With  $n_{\parallel}/n_{\perp} = 1.3$ , the right-hand side of the equation has the value of  $\sim 0.8$ . This value is in reasonable agreement with the effective mass parameters obtained. The data of  $\alpha_{\parallel}/\alpha_{\perp}$  for room temperature are subject to error, as mentioned previously, and a reliable check of this equation cannot be made.